Structural Eng./Earthquake Eng., JSCE, Vol. 17, No. 2, 175s-185s, 2000 July
(J. Struct. Mech. Earthquake Eng., JSCE, No. 654/ I-52)

MACRO-MICRO ANALYSIS FOR PREDICTION OF STRONG MOTION DISTRIBUTION IN METROPOLIS

Tsuyoshi ICHIMURA [1]and Muneo HORI[2]

[1]Member of JSCE, M. Eng., Postgraduate Student, Earthquake Research Institute, University of Tokyo
(Yayoi, Bunkyo, Tokyo 113-0032, Japan)
[2]Member of JSCE, Ph. D., Associate Professor, Earthquake Research Institute, University of Tokyo
(Yayoi, Bunkyo, Tokyo 113-0032, Japan)

This paper proposes a macro-micro analysis for the prediction of a strong motion distribution in a metropolis. The analysis uses the singular perturbation expansion and the bounding media theory, to reduce required numerical computation and to consider the uncertainty of ground and geological structures. A prototype of the numerical code for the macro-micro analysis is developed, and an actual earthquake is simulated. The comparison with measured data supports the basic validity of the proposed method.

Key Words *: macro-micro analysis, singular perturbation expansion, bounding media theory*

1. INTRODUCTION

The prediction of the strong motion distribution is of major importance in planning countermeasures for a huge earthquake, which could happen in a metropolis. Higher spatial and time resolution is desirable. For practical purposes, the time resolution up to the order of 0.1 [sec] is needed, and hence, the spatial resolution up to the order of 1.0 [m] is needed. Hence, we are considering to numerically simulate wave propagation processes from a fault to a target site.

There are two difficulties in the numerical simulation of such wave propagation processes, the requirement of huge computer resources and the uncertainty of ground and geological structures. The first difficulty is easily understood if the wave propagation in a cube of the order of $10\times10\times10$[km] for a time duration of 40[sec] is simulated. **Table 1** shows a rough estimate of the amount of memory required for a finite difference method (FDM), a finite element method (FEM) and a boundary element method (BEM) to solve this problem with the spatial resolution of 10[m] and the time resolution of 0.1[sec]. Although the BEM appears acceptable, it must run a large number of computation steps, which increases, almost proportionally to the square of the element number. The second difficulty may be more serious, since accurate modeling is essential for a reliable simulation. Available information, however, is always limited for the underground structures of the metropolis. Because of these two difficulties, the latest numerical analysis at the present date can assure the precision of the computation with the time resolution up to 0.9[sec][1] only.

Table 1 Estimate of required memory for numerical simulation

	FDM	FEM	BEM
memory[MB]	5×10^3	5×10^3	1

In this paper, we propose a new analysis method for the simulation of the wave propagation process in a metropolis[2), 3), 4)]. This method, called a *macro-micro analysis*, solves the above two difficulties by taking advantage of the singular perturbation which leads to a multi-scale analysis to achieve high spatial and time resolution and the bounding media theory

which provides optimistic and pessimistic evaluation depending on the uncertainty of the ground structure[5),6),7)]. In this macro-micro analysis, the metropolis is modeled as a statistically varying heterogeneous body which is constructed by using boring data measured on several hundred (or thousand) points and interpolating them with some variances. The bounding media theory then determines two fictitious but deterministic media such that optimistic and pessimistic evaluations are made for the expectation of the strong motion distribution. The wave propagation processes in these media are analyzed by taking the singular perturbation expansion of a displacement field. The first-order solution is computed for a whole city with lower resolution (macro-analysis), and the second-order solution is obtained for some smaller zones with higher resolution (micro-analysis), and hence they lead to an efficient multi-scale analysis.

The main objectives of the present paper are 1) to rigorously establish a new theory of the macro-micro analysis, 2) to carry out numerical experiments to develop a computer code of the macro-micro analysis, and 3) to verify the basic validity of the analysis method comparing with observed data. The comparison uses a strong motion record obtained in Yokohama City. Note that this paper uses index notation, denotes the differentiation with respect to the x_i coordinate by d_i (i.e., $\mathrm{d}_i = \partial/\partial x_i$), and employs the summation convention.

2. FORMULATION

For simplicity, we assume that a metropolis consists of elastic materials and denote it by V. This V has distinct sub-domains ω^α (α = 1, 2, $\cdots$, N), and the uncertainty of heterogeneous ground and geological structures is regarded as a statistical distribution[8)] of the material properties in each ω^α. That is, assuming the isotropy, we set Young's modulus, E, varies in ω^α according to a suitable probability distribution function φ^α; the Poisson ratio is assumed to be constant throughout V; see **Fig. 1**. We introduce a non-dimensional parameter, ε ($\ll$ 1), as the relative size of the heterogeneity to V, and denote the

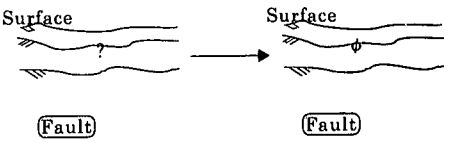

Fig. 1 modeling of meteropolis

elasticity tensor and density fields of V by

$$c^\varepsilon_{ijkl}(\mathbf{x}) \text{ and } \rho^\epsilon(\mathbf{x})$$

where $\mathbf{x}$ stands for the position vector. The governing equations for a displacement field, u^ε_i, are

$$\mathrm{d}_i(c^\varepsilon_{ijkl}(\mathbf{x})\mathrm{d}_l u_k(\mathbf{x},t)) - \rho^\epsilon(\mathbf{x})\ddot{u}_j(\mathbf{x},t) = 0. \quad (1)$$

To show the bounding media, we first consider the quasi-static deformation of V, neglecting the inertia terms, i.e.,

$$\mathrm{d}_i(c^\varepsilon_{ijkl}(\mathbf{x})\mathrm{d}_l u^\varepsilon_k(\mathbf{x})) = 0. \quad (2)$$

For one realization of c^ε_{ijkl}, we can find two approximate solutions which bound the total strain energy stored in V. These bounds are derived from the generalized[5),6)] Hashin-Shtrikman variational principle (HSVP), and, denoting the strain energy by $e(\mathbf{c}^\varepsilon)$, we can compute the bounds as follows:

$$e^{o+} - J(\mathbf{s}^*;\mathbf{c}^\varepsilon;\mathbf{c}^{o+}) < e(\mathbf{c}^\varepsilon) < e^{o-} - J(\mathbf{s}^*;\mathbf{c}^\varepsilon;\mathbf{c}^{o-}). \quad (3)$$

Here, $e^{o\pm}$ is the total strain energy when V consists of uniform elasticity, $c^{o\pm}_{ijkl}$, which makes $c^\varepsilon_{ijkl} - c^{o\pm}_{ijkl}$ positive- and negative-definite, and J is a functional for eigen-stress s^*_{ij} defined as

$$J(\mathbf{s}^*;\mathbf{c}^\varepsilon;\mathbf{c}^o) = \int_V \frac{1}{2} s^*_{ij}((c^\varepsilon_{ijkl} - c^o_{ijkl})^{-1} s^*_{kl} - \epsilon^d_{ij}(\mathbf{s}^*) - 2\epsilon^h_{ij})\, \mathrm{d}V. \quad (4)$$

where ϵ^d_{ij} is the strain due to $\mathbf{s}^*_{ij}$; see APPENDIX A. When c^ε_{ijkl} varies, we can define two media using Eq. (3) such that the media provide upper and lower bounds for the expectation of the strain energy. Indeed, since Eq. (3) holds for any s^*_{ij}, the average of the right and left sides with respect to φ^α's of all sub-domains are the bounds. Putting an overbar on an averaged quantity, we can compute the bounds as

$$\overline{J(\mathbf{s}^*;\mathbf{c}^\varepsilon;\mathbf{c}^{o\pm})} = \int_V \frac{1}{2} s^*_{ij}(\overline{(c^\varepsilon_{ijkl} - c^o_{ijkl})^{-1}} s^*_{kl} - \epsilon^d_{ij}(\mathbf{s}^*) - 2\epsilon^h_{ij})\, \mathrm{d}V. \quad (5)$$

It is easily shown that as c^{o+}_{ijkl} vanishes or as c^{o-}_{ijkl} increases unboundedly, $\overline{(c^{\epsilon}_{ijkl} - c^{o+}_{ijkl})^{-1}}$ approaches $(\overline{c}^{+}_{ijkl} - c^{o+}_{ijkl})^{-1}$ with

$$\overline{c}^{+}_{ijkl}(\mathbf{x}) = \left(\int \varphi^{\alpha}(E)(c^{\epsilon}_{ijkl})^{-1}(\mathbf{x}; E)\, \mathrm{d}E \right)^{-1}, \tag{6}$$

or $(\overline{c}^{-}_{ijkl} - c^{o-}_{ijkl})^{-1}$ with

$$\overline{c}^{-}_{ijkl}(\mathbf{x}) = \int \phi(E) c^{\epsilon}_{ijkl}(\mathbf{x}; E)\, \mathrm{d}E, \tag{7}$$

respectively. Therefore, we can derive the following inequality for $\overline{e}$:

$$e^{o+} - J(\mathbf{s}^*; \overline{\mathbf{c}}^{+}; \mathbf{c}^{o+}) \;<\; \overline{e} \;<\; e^{o-} - J(\mathbf{s}^*; \overline{\mathbf{c}}^{-}; \mathbf{c}^{o-}). \tag{8}$$

By definition, J yields the sharpest bound for $\overline{e}$ for eigen-stress that solves a boundary value problem of a body with $\overline{c}^{\pm}_{ijkl}$. In other words, the two fictitious but deterministic media given by $\overline{c}^{\pm}_{ijkl}$ provide bounds for the expectation of the strain energy of statistically varying V. These media, denoted by $V^{\pm}$ are called *bounding media*; see **Fig. 2**.

When $\overline{c}^{\pm}_{ijkl}$ requires a huge number of discretization, the numerical computation becomes tremendous. For a smarter computation, we apply the singular perturbation of u^{ϵ}_i, introducing a slow spatial variable, $\mathbf{X} = \varepsilon\mathbf{x}$,

$$u^{\epsilon}_i(\mathbf{x}) \;\approx\; u^{(0)}_i(\mathbf{X}, \mathbf{x}) + \varepsilon u^{(1)}_i(\mathbf{X}, \mathbf{x}) + \cdots. \tag{9}$$

Here, $\mathbf{X}$ varies in V and $\mathbf{x}$ in a small domain around $\mathbf{X}$. The derivative with respect to x_i can be replaced by $\mathrm{d}_i + \varepsilon \mathrm{D}_i$ ($\mathrm{D}_i = \partial/\partial X_i$). We can obtain the following expansion of Eq. (2) in terms of $u^{(0)}_i$ and $u^{(1)}_i$:

$$\begin{aligned}
&\varepsilon^0(\mathrm{d}_i(\overline{c}^{\pm}_{ijkl}\mathrm{d}_l u^{(0)}_k)) \\
&+ \varepsilon^1(\mathrm{d}_i(\overline{c}^{\pm}_{ijkl}(\mathrm{d}_l u^{(1)}_k + \mathrm{D}_l u^{(0)}_k)) + \mathrm{D}_i(\overline{c}^{\pm}_{ijkl}\mathrm{d}_l u^{(0)}_k)) \\
&+ \varepsilon^2(\mathrm{D}_i(\overline{c}^{\pm}_{ijkl}(\mathrm{d}_l u^{(1)}_k + \mathrm{D}_l u^{(0)}_k)) \\
&\quad + \mathrm{d}_i(\overline{c}^{\pm}_{ijkl}(\mathrm{d}_l u^{(2)}_k + \mathrm{D}_l u^{(1)}_k))) + O(\varepsilon^3) = 0.
\end{aligned}$$

To make the coefficients of ε^0 and ε^1 always vanish, we set that $u^{(0)}_i$ is a function of $\mathbf{X}$ only and that $u^{(1)}_i$ is of the form

$$u^{(1)}_i(\mathbf{X}, \mathbf{x}) = \chi^{(1)}_{ipq}(\mathbf{X}, \mathbf{x}) \mathrm{D}_q u^{(0)}_p(\mathbf{X})$$

where $\chi^{(1)}_{ipq}$ satisfies

$$d_i\left(\overline{c}^{\pm}_{ijkl}(\mathbf{X}, \mathbf{x})(d_l \chi^{(1)}_{kpq}(\mathbf{X}, \mathbf{x}, t) + I_{klpq})\right) = 0, \tag{10}$$

with I_{ijkl} being a fourth-order (symmetric) identity tensor. Taking the volume average over $\Omega_{\mathbf{X}}$, denoted by $\langle(.)\rangle$, for the coefficient of ε^2, we obtain

$$D_i\langle\overline{c}^{\pm}_{ijpq}(d_q \chi^{(1)}_{pkl} + I_{pqkl})\rangle D_l u^{(0)}_k = 0. \tag{11}$$

Equations (10) and (11) are the governing equations for $u^{(0)}_i$ and $u^{(1)}_i$.

Boundary conditions are required to determine $\chi^{(1)}_{ipq}$ in $\Omega_{\mathbf{X}}$. Such conditions, however, cannot be determined unless u_i is obtained in V. Instead of exact boundary conditions, we use the homogeneous strain and stress boundary conditions, $u_i = x_j E_{ji}$ and $t_i = n_j \Sigma_{ji}$ with constant E_{ij} and Σ_{ij}, since they bound the strain energy of $\Omega_{\mathbf{X}}$ subjected to various boundary conditions, i.e.,

$$\langle\frac{1}{2}\epsilon^{E}_{ij}\overline{c}^{\pm}_{ijkl}\epsilon^{E}_{kl}\rangle \;\le\; \langle\frac{1}{2}\epsilon^{G}_{ij}\overline{c}^{\pm}_{ijkl}\epsilon^{G}_{kl}\rangle \;\le\; \langle\frac{1}{2}\epsilon^{\Sigma}_{ij}\overline{c}^{\pm}_{ijkl}\epsilon^{\Sigma}_{kl}\rangle, \tag{12}$$

where superscripts E, G, and Σ stand for strains due to homogeneous strain, general, and homogeneous stress boundary conditions, respectively, satisfying $\langle\epsilon^{E}_{ij}\rangle = \langle\epsilon^{G}_{ij}\rangle = \langle\epsilon^{\Sigma}_{ij}\rangle$. Putting the superscripts E and Σ, we rewrite Eq. (11) as

$$\mathrm{D}_i(C^{E,\Sigma}_{ijkl}\mathrm{D}_l u^{(0)E,\Sigma}_k(\mathbf{X})) = 0, \tag{13}$$

where

$$C^{E,\Sigma}_{ijkl} = \langle\overline{c}^{\pm}_{ijpq}(d_q \chi^{(1)E,\Sigma}_{pkl} + I_{pqkl})\rangle. \tag{14}$$

Finally, we consider a dynamic case when the inertia effects are included. If waves of smaller frequencies are dominant, the bounding media $V^{\pm}$ for the quasi-static case can be used to obtain approximate solutions (It is certainly possible to define bounding media considering inertia effects rigorously. The formulation of these media is essentially the same as that in the quasi-static case.). Indeed, the governing equations for the first term in the expansion are

$$D_i(C^{E,\Sigma}_{ijkl}(\mathbf{X})D_l u^{(0)}_k(\mathbf{X}, t)) - R(\mathbf{X})\ddot{u}^{(0)}_j(\mathbf{X}, t) = 0, \tag{15}$$

where $C^{E,\Sigma}_{ijkl}$ is the effective elasticity tensor of the (quasi-static) $V^{\pm}$ and R is the effective density given as $R = \langle\overline{\rho}\rangle$.

Since the regular perturbation does not lead to the coupling of terms in different orders, we introduce a slow time variable, $T = \sqrt{\varepsilon}t$, and take

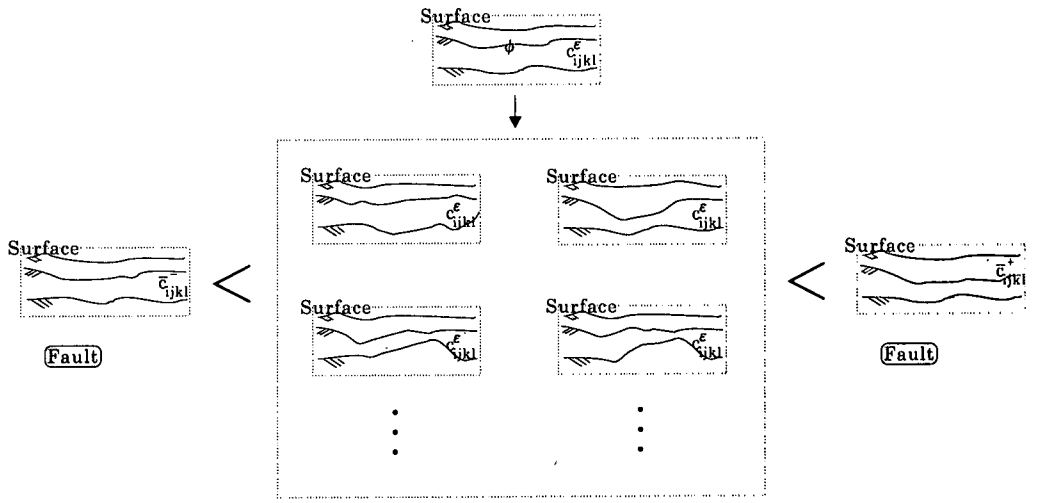

Fig. 2 Bounding media

the singular perturbation with respect to time as well as space, i.e.,

$$u_i^\varepsilon(\mathbf{x},t) \approx u_i^{(0)}(\mathbf{X},T) + \varepsilon u_i^{(1)}(\mathbf{X},\mathbf{x},T,t) + \cdots. \tag{16}$$

Substitution of this expansion into Eq. (1) leads to expressions similar to the quasi-static case, and derives the governing equation for the second term as

$$d_i(\bar{c}^{\pm}_{ijkl}(\mathbf{X},\mathbf{x})(d_l u_k^{(1)}(\mathbf{X},\mathbf{x},T,t) + D_l u_k^{(0)}(\mathbf{X},T))) - \bar{\rho}(\mathbf{X},\mathbf{x})\frac{\partial^2 u^{(1)}}{\partial t^2}(\mathbf{X},\mathbf{x},T,t) = 0. \tag{17}$$

These equations are essentially the same as a case when $u_i^{(1)}$ is regarded as scattered waves due to the local heterogeneity when $u_i^{(0)}$ is given as an incident wave (If another time scale is used, the resulting equations are different; for instance, $T' = \varepsilon t$ naturally leads to the damping in the larger spatial and slower time scales.).

As is seen, the macro-micro analysis leads to two approximate solutions for wave propagation processes in a metropolis with uncertain underground structures. These solutions are for fictitious bounding media and computed by using the singular perturbation method. By definition, the approximate solutions given by the bounding media can provide bounds for the expectation of the total energy stored in the metropolis, and local responses may not be bounded. However, we may expect that the bounding media can bound local quantities such as velocity as it is related to the local energy.

Table 2 Material properties

	ρ[kg/m^3]	C_2[m/sec]	ν
upper layer	2000.	120.	0.27
lower layer	3000.	3500.	0.27

3. NUMERICAL EXPERIMENT

While the macro-micro analysis solves the two major difficulties by respectively computing $u_i^{(0)}$ in the macro-analysis and $u_i^{(1)}$ in the micro-analysis, some cares must be taken for the numerical computation. This section presents results of numerical experiments made to this end, in which a simple problem is solved as an example; **see Fig. 3**. The material and source parameters are summarized in **Tables 2** and **3**. A point source model with a ramp function is used; the fault area is 2.19[km^2], the dislocation gap is 0.3[m], and the rise time[9] is 0.64[sec].The experiments use a DEC-10 Alpha PC164LX with 512MB memory, and the Bi-CGSTAB method[10] is used in solving large-scale matrix equations.

(1) Macro-Analysis

We use the BEM[11),12),13),14)] for the macro-analysis since it can easily handle open bound-

Table 3 Properties of source

Lat.	Long.	Depth	Strike	Dip	Rake	Mag.
35.6N	140.0E	76km	10°	62°	100°	4.7Mw

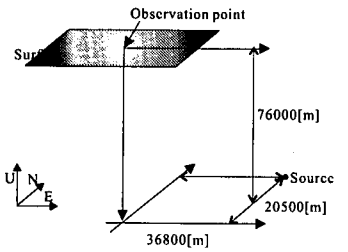

Fig. 3 Model used for numerical experiments

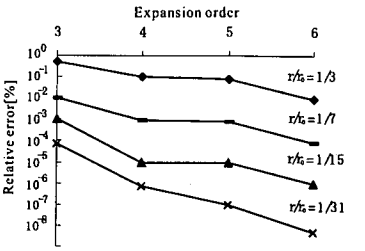

Fig. 4 Relative error of computing Green function

ary conditions and requires smaller amount of memories; see **Table 1**. While the fast Fourier transform method is used and frequency domain problems are solved, the numerical computation is still huge as a large-scale discretization is needed. To overcome this problem, we apply a fast multi-pole method (FMM)[4),15),16),17),18)], which approximately solve the problem drastically reducing numerical computation required for the BEM. The key points of the FMM are 1) to efficiently compute Green's function by expanding it in Taylor series and 2) to make smart matrix computation through the clustering. The clustering means that for given arrangement of meshes, each mesh is regarded as an element of the smallest level, a set of some neighboring meshes as one element of the second smallest level, and so on. The matrix algebra for each mesh is efficiently transformed to matrix algebra for elements of several levels; see APPENDIX B for a more detailed explanation. It should be mentioned that Taylor series expansion of Green's function could be made automatically by using, say, MATHEMATICA, even though the function is complicated.

The accuracy of approximate solutions given by the FMM mainly depends on the order of the Taylor expansion and the clustering; see APPENDIX B. Since there is a trade-off between the accuracy and the efficiency, we choose suitable the expansion order and the clustering. Since the macro-analysis is aimed at the time resolution around 1.0[Hz], the accuracy of computing Green's function with the FMM up to this order is first examined. The results are shown in **Fig. 4**; the expansion order means the highest derivative with respect to each coordinate, r/r_0 stands for the size of clusters, and the relative error is the maximum value of relative errors with respect to the exact value during the event (A larger value of r/r_0 means more meshes are used in forming one cluster.). It is seen that, in order for the relative error to be less than 0.1%, the expansion order is at least 4 when the cluster size is 1/3. Next, we check the accuracy of computing waves from the comparison with the waves obtained by using a standard BEM. **Fig. 5** shows the error at a center point when the model is discretized into 8×8 meshes; the relative error is the error of the approximated displacement with respect to the exact one. It is seen that the accuracy is satisfactory, even though it is slightly worse than the accuracy of computing Green's function.

Since the accuracy is secured, we examine the numerical efficiency of the FMM. The CPU times of the BEM with/without the FMM for various sizes of descritization are shown in **Fig. 6**; CPU time is for the matrix computation only. Such efficiency enables us to compute a descritization when the model is decritized into 128×128 meshes with 50×50[m]. The standard BEM is not capable of computing this setting. The computed displacement shown in **Fig. 7**; the FMM succeeds in catching the arrival of the primary wave clearly even for such a large-scale computation.

(2) Micro-Analysis

We apply the FEM[19)] for the micro-analysis, since it is suitable to compute the wave propagation processes through highly heterogeneous ground structures. Furthermore, the FEM will

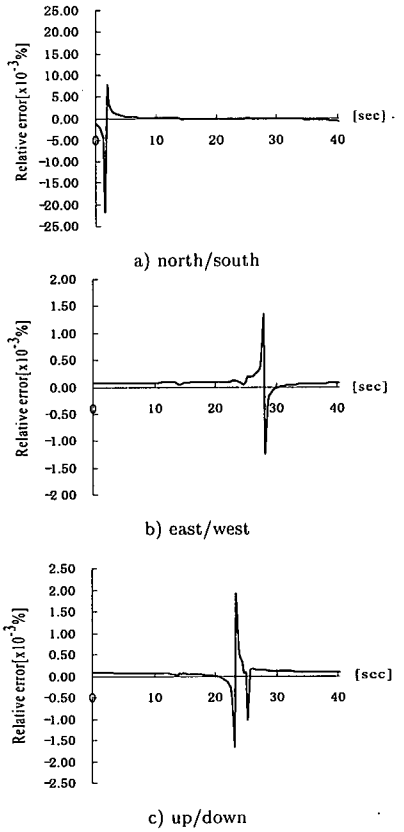

Fig. 5 Relative error of BEM with FMM

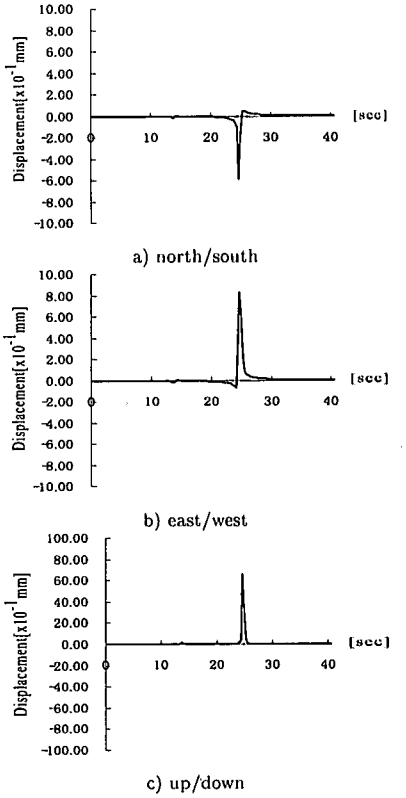

Fig. 7 Computed profile of displacement

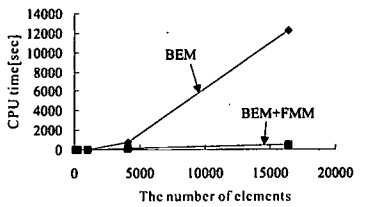

Fig. 6 CPU time for matrix computation

be applicable to a case when non-linear responses of soils need to be accounted for. The major difficulty in solving dynamic problems with the FEM is the treatment of artificial boundary, which is introduced to make a target body finite. Besides, in the present formulation, the second order solution, $u_i^{(1)}$, should not produce any reflection to the surrounding media, since a target of the micro-analysis is regarded as a small sub-domain embedded in a large medium which is computed in the macro-analysis. We put a layer around the sub-domain to eliminate reflection there such the sub-domain is surrounded by a large domain. We use tuned Rayleigh dampers for the layer, which can cut waves going out more or less normal to the boundary.

The properties of the Rayleigh dampers (the damping matrix) must be determined through trial-and-error. We apply the micro-analysis to the previous example to this end. A homogeneous sub-domain to which the micro-analysis is applied is shown in **Fig. 8b)**, when the incident wave ($u_i^{(0)}$) is computed for a domain shown in **Fig. 8a)**; see **Tables 2** and **3** for the material and source parameters. A point source model with a ramp function is used; the fault area is 2.19[km^2], the dislocation gap is 0.3[m], and the rise time[9] is 0.64[sec]. It is shown that two distinct layers of the Rayleigh dampers are sufficient when the sub-domain of 40×40×40[m] is descritized by elements of 2×2×2[m] (It is certainly true that thicker layers are better to cut unnecessary reflected waves. However, they result in larger numerical computation.). The inner and outer layers have damper matrices, $[C] = 1.[M]$[kg/sec] and $10.[M]$[kg/sec], respectively. The trial-and-

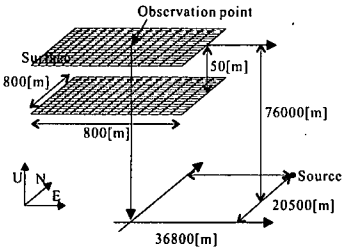

a) model for macro-analysis

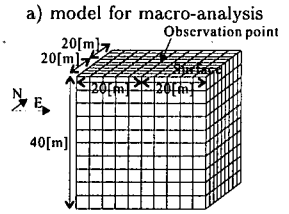

b) model for micro-analysis

Fig. 8 Model for numerical experiment

error is made to minimize scattered waves ($u_i^{(1)}$) when the first order solution ($u_i^{(0)}$) is put into a sub-domain which is set to be homogeneous. In **Fig. 9**, the wave profiles of both $u_i^{(0)}$ and $u_i^{(0)} + \varepsilon u_i^{(1)}$ are plotted. As is seen, these wave profiles are almost identical, and the maximum relative error is less than 0.1%.

4. RESULTS AND DISCUSSIONS

In order to verify its basic validity of the proposed analysis method, we try to simulate actual an earthquake and compare the results with observed data. The properties of the target earthquake are summarized in **Table 4**. A point source model with a ramp function is used; the fault area is 3.8[km^2], the dislocation gap is 0.47[m], and the rise time[9] is 0.64[sec]. Data measured at the Chitose Park (35.4338N, 139.6372E) in Yokohama City are used for the comparison. Due to the limitation of computational resources, we use a simple parallel two-layer structure shown in **Fig. 10** to model the geological structure near the observation point; the top and bottom layers correspond to the surface grounds and the base, respectively. **Table 5** presents the properties of the bottom layer. For the more complicated top layer, **Figs. 11** and **12** together with **Table 6** show the ground structures and the material properties; a number (401~414) in **Fig. 11**

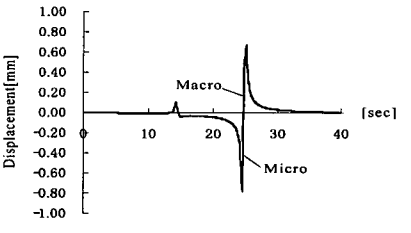

a) north/south

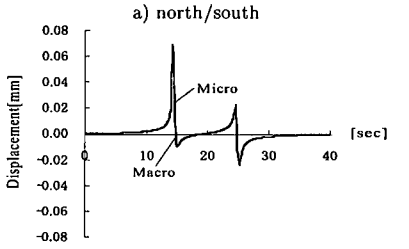

b) east/west

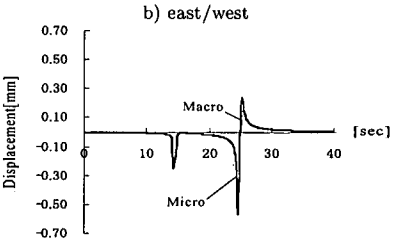

c) up/down

Fig. 9 Wave profile computed by micro-analysis

Table 4 Properties of earthquake

Lat.	Long.	Depth	Strike	Dip	Rake	Mag.
35.6N	140.0E	56km	213°	66°	-151°	5.3Mw

Table 5 Properties of bottom layer

ρ[kg/m^3]	C_2[m/sec]	ν
2500.	3500.	0.27

indicates boring data shown in **Fig. 12**, and a character ($Ac_{1,2}$, As_2, T) in **Fig. 12** is a sub-layer referred in **Table 6** in which the material properties are presented.

First, we determine a stochastic body for a region around the observation point. Assuming that the bottom layer is deterministic, we set variances of 10% for each sub-layers a top layer which is now modeled as a heterogeneous domain of 400×400×50[m] around the observation point and determine ground structures through the linear interpolation. Two bounding media are de-

Table 6 Properties of top layer

	ρ[kg/m^3]	C_2[m/sec]	ν
Ac_1	1500.	100.	0.27
Ac_2	1600.	140.	0.27
As_2	1800.	210.	0.27
T	2100.	700.	0.27

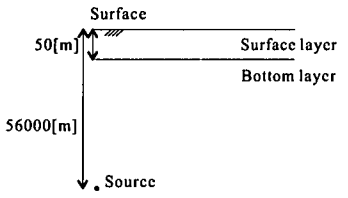

Fig. 10 Geological structure

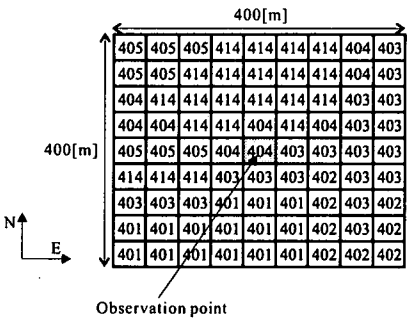

Fig. 11 Structure of top layer

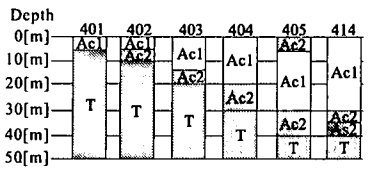

Fig. 12 Soil structure

termined for this domain, and **Table 7** summarizes the material properties which are easily obtained by assuming uniform strain or stress state. Next, we compute the wave propagation process in these media for the time duration of 40.96 [sec] with the time increment of 0.32 [sec]. The model used for the macro-analysis is shown in **Fig. 13a)**. The ground surface and the interface are of 800×800[m], and are divided into 16×16 elements. It should be mentioned that some care must be taken in solving the resulting matrix equation since the contrast in the material properties between the top and bottom layers is quite high. We apply the sub-structure method which is often used in the FEM; see APPENDIX C for the detailed explanation. The micro-analysis is applied to one sub-domain of 40×40×40[m] in the top layer, and cubic elements of 2×2×2[m] are used for the descritization; see **Fig. 13b)**.

The displacement computed by the macro-analysis is in **Fig. 14**. The acceleration computed by the micro-analysis during 1.0 [sec] after the arrival of the main shock is plotted in **Fig. 15** (The value of ε is set as 0.04, as the ratio of the element scale in the macro- and in micro-analysis.). These displacement and acceleration are at the observation point, which is located in the center of the surface. It should be noted that the results of the micro-analysis is computed up to 5.0[Hz] as the present analysis assures the precision of computation only to this frequency. The displacement waveform in the optimistic and pessimistic cases resembles very well each other. The maximum value of the displacement amplitude, however, is different for 11.8% in the maximum between the optimistic case and the pessimistic case. The profile of the computed acceleration is different from that of the measured one, mainly because the fault mechanism is modeled in the simplest manner. However, the magnitude of the computed acceleration is of the same order as that of the measured one. These results support the basic validity of the proposed method.

In the present simulation, the two bounding media do not bound the acceleration which were locally measured. However, they may provide optimistic and pessimistic estimates on local quantities such as the maximum acceleration; see **Fig. 15**. As an illustrative example, we present the distribution of the maximum value of computed acceleration in each direction at 20×20[m] region around the observation point in **Fig. 16** for the optimistic and pessimistic cases, respectively. The spatial resolution is 2.0[m]. The macro-analysis cannot tell the difference in this resolution, and the distribution becomes almost uniform. Due to the local ground structures, the micro-analysis can produce some local concentration. It should be emphasized that the validity of these results shown in **Fig. 16** can not be verified

Table 7 Properties of bounding media

	ρ[kg/m^3]	C_2[m/sec]	ν
V^+	1796.6	451.5	0.27
V^-	1783.6	319.1	0.27

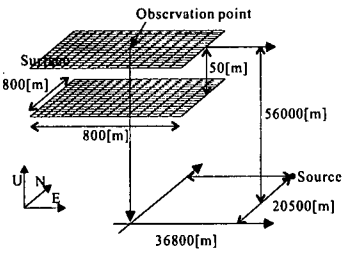

a) model for macro-analysis

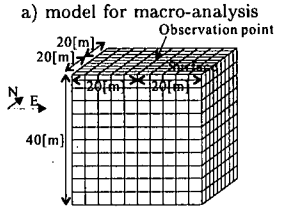

b) model for micro-analysis

Fig. 13 Model for numerical simulation

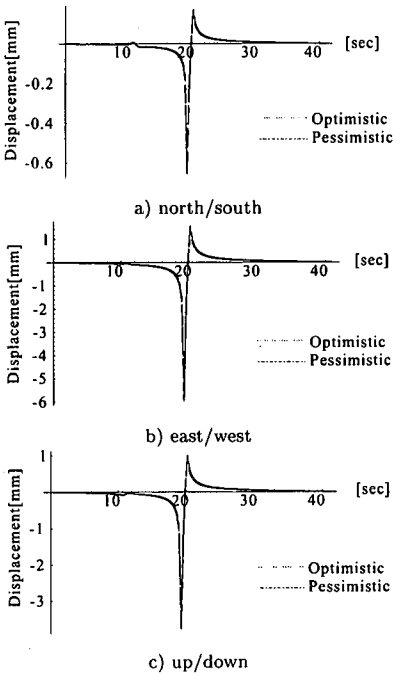

a) north/south

b) east/west

c) up/down

Fig. 14 Displacement computed by macro-analysis

by the measured data at all. However, they suggest the potential usefulness of the present analysis method.

5. CONCLUDING REMARKS

The basic validity of the macro-micro analysis is verified through the comparison of actual data; it might be remarkable that the computed waves are of the same order as the observed one even though the simplest model was used. While further investigation is inevitable, we can expect some potential usefulness of the proposed method. At this stage, we are planning to compare the numerical simulation with observed data in a wider region in respect of the maximum value and the waveform; for instance, the whole Yokohama City is a candidate. The validity of optimistic and pessimistic estimates of some local quantities will be focused, in order to examine the practical application of the bounding media theory when a metropolis is statistically modeled.

ACKNOWLEDGEMENT: In this paper, we use K-net and FREESIA data, which is published by NIED (National Research Institute for Earth Science and Disaster Prevention). I thanks three anonymous reviewers for constructive comments, which also significantly improved the manuscript. The primary author is the Japan Soc. for the Promotion of Sci. special researcher. This study is receiving the assist of the Ministry of Education grant-in-aids for Scientific Research (fellowship for encouraging special researchers No.10015).

APPENDIX A HSVP

The HSVP is based on the equivalent inclusion method which replace Eq. (2) as

$$c^{\circ}_{ijkl}\mathrm{d}_l\mathrm{d}_i u^{\epsilon}_k(\mathbf{x}) + \mathrm{d}_i\sigma^*_{ij}(\mathbf{x}) = 0, \qquad \text{(A.1)}$$

$$\sigma^*_{ij}(\mathbf{x}) = (c^{\epsilon}_{ijkl}(\mathbf{x}) - c^{\circ}_{ijkl})\frac{1}{2}(\mathrm{d}_l u^{\epsilon}_k(\mathbf{x}) + \mathrm{d}_k u^{\epsilon}_l(\mathbf{x})).$$

Here, σ^*_{ij} is called eigen-stress. For a given σ^*_{ij} and given suitable boundary conditions, the solution of the first equation is formally expressed as $u^h_i + u^d_i$, where u^h_i and u^d_i are displacement in the absence and the presence of σ^*_{ij}. Then, the second equation is replaced by

$$(c^{\epsilon}_{ijkl}(\mathbf{x}) - c^{\circ}_{ijkl})^{-1}\sigma^*_{kl}(\mathbf{x}) - \epsilon^h_{kl}(\mathbf{x}) + \epsilon^d_{kl}(\mathbf{x}, \sigma^*). \qquad \text{(A.2)}$$

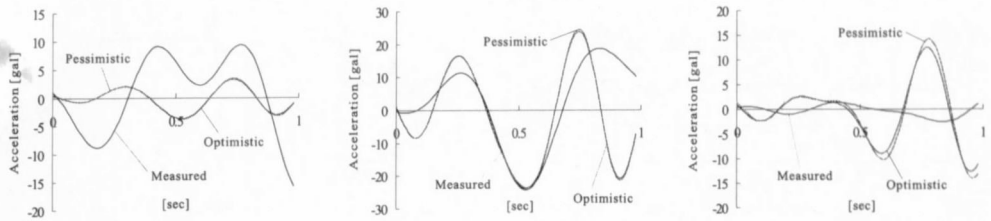

a) north/south b) east/west c) up/down

Fig. 15 Acceleration computed by micro-analysis

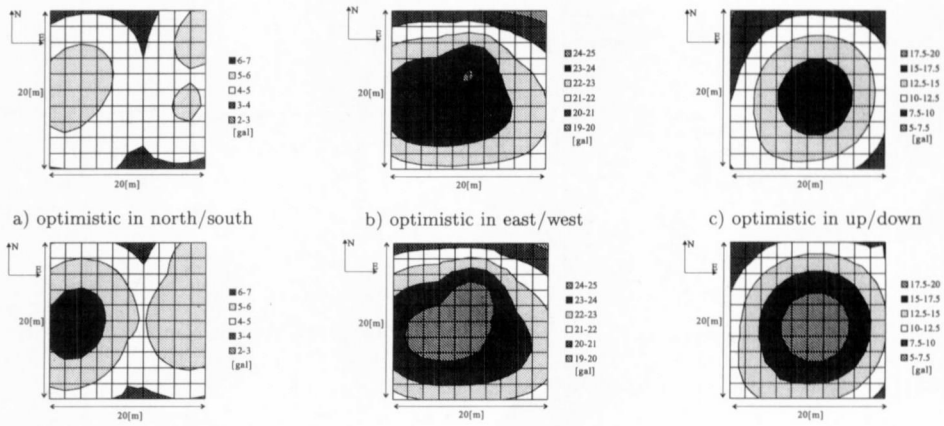

a) optimistic in north/south b) optimistic in east/west c) optimistic in up/down

d) pessimistic in north/south e) pessimistic in east/west f) pessimistic in up/down

Fig. 16 Distribution of maximum acceleration

We can define a functional, J given by Eq. (4), such that the Euler equations coincide with Eq. (A.2). This functional has the following two properties: 1) J gives e for the exact eigen-stress that stationarizes J, as $J(\sigma^*) = e - e^{\mathrm{o}}$. and; 2) for c^{o}_{ijkl} making $c_{ijkl} - c^{\mathrm{o}}_{ijkl}$ positive- or negative-definite, the stationary value of J is the minimum or maximum, respectively. It follows from the above properties that the total strain energy of V is bounded by Eq. (3).

APPENDIX B FMM

In terms of Green's function, G, an effect of sources which are distributed on a surface S upon the origin is formally expressed as

$$\int_S G(0,0,0;x,y,z) u(x,y,z)\, dS.$$

The FMM (Strictly speaking, this method ought to be called a panel clustering method.) efficiently[16] computes this surface integral. The Taylor expansion of G around, say, a point (x_0, y_0, z_0), yields

$$\sum_{k=0}^{\infty}\sum_{l=0}^{\infty}\sum_{m=0}^{\infty} \times \int_S (x-x_0)^k\ (y-y_0)^l\ (z-z_0)^m\ u(x,y,z) dS \times \frac{1}{k!\ l!\ m!} \left.\frac{\partial^{(k+l+m)} G(0,0,0;x,y,z)}{\partial x^k\ \partial y^l\ \partial z^m}\right|_{(x_0,y_0,z_0)}.$$

The coefficients of Green's function can be obtained through MATHEMATICA, and a truncated sum can provide an accurate value if the sources are relatively far.

When S is divided into several subsurfaces, S_i's, the surface integral of polynomials derived from the Tayler expansion becomes

$$\sum_{i=1}\sum_{k'=0}^{\infty}\sum_{l'=0}^{\infty}\sum_{m'=0}^{\infty} \binom{k}{k'}\binom{l}{l'}\binom{m}{m'} \times \int_{S_i} (x-x_i)^{k'}\ (y-y_i)^{l'}\ (z-z_i)^{m'}\ u(x,y,z)\, dS_i \times (x_i-x_0)^{k-k'}\ (y_i-y_0)^{l-l'}\ (z_i-z_0)^{m-m'},$$

where (x_i,y_i,z_i) is a point at the center of S_i. This expression means that the integration over S is given by combining the integration over smaller sub-surfaces. This method is called clustering, and can reduce the numerical computation drastically.

APPENDIX C SUB-STRUCTURE METHOD

The two layered model used in Section 4 has high contrast in material properties between the top and bottom layers. Since the iteration method is used as a solver, the BEM cannot solve the resulting matrix equation well. The sub-structure method is thus introduced, such that the convergence is guaranteed even for such a model. The procedure of the sub-structure method is summarized as follows: 1) divide a whole domain into several distinct layers; 2) generate a solution satisfying the compatibility across the boundaries of the layers; and 3) repeat the second procedure until the solution converges. In this way, the sub-structure method can fasten the convergence of the solution. It should be noted that memories required to save matrix and vector components are reduced as the matrix equation in each layer is separately computed.

REFERENCES

1) Hesheng Bao, Jacobo Bielak, Omar Ghattas, Loukas F. Kallivokas, David R. O'Hallaron, Jonathan R. Shewchuk, and Jifeng Xu : Large-scale Simulation of Elastic Wave Propagation in Heterogeneous Media on Parallel Computers. *Computer Methods in Applied Mechanics and Engineering 152(1-2)*, pp.85-102, 22 January 1998.
2) Ichimura, T. and Hori, M. : Macro-Micro Analysis for Prediction of Strong Motion Distribution in Large City, *Journal of Applied Mechanics*, vol.1, pp.607-612, 1998.
3) Ichimura, T. and Hori, M. : Macro-Micro Analysis for Prediction of Strong Motion Distribution in Large City, *Symp. for Disaster by a Huge Earthquake in Large City*, pp.123-124, 1998 (in Japanese).
4) Ichimura, T. : Basic Research for Simulator of Strong Motion Distribution, graduate thesis Department of Civil Engineering in the University of Tokyo, 1998.
5) Hori, M. : Bounds for Effective Material Properties of Statistically Non-homogeneous Solid, *Structual Eng./Earthquake Eng.* vol.11, No.3, pp.131-140, October 1994
6) Hori, M. and Nemat-Nasser, S. : On Two Micromechanics Theories for Determining Micro-Macro Relations (to be published).
7) Yuge, K. and Kikuchi, N. : Analysis of a Composite Beam by the Homogenization Method, *Jounal of Applied Mechanics*, vol.1, pp.203-213, 1998.8.
8) Andre G. Journel: Fundamentals of geostatistics in five lessons, American Geophysical Union, 1989.
9) Kikuchi, M. and Ishida, M.: Source Retrieval for Local Earthquakes with Broadband Records, *Bull. Seism. Soc. Am.*, 83, pp.330-346, 1993.
10) van der Vorst, H.A. : BI-CGSTAB:A Fast and Smoothly Converging Variant of BI-CG for the Solution of Non symmetric Linear Systems. *SIAMJ. Stat. Comput.*, No.2 (March,1992), pp.631-644.
11) Guiggiani, M. and Gigante, A. : A General Algorithm for Multidimensional Cauchy Principal Value Integrals in the Boundary Element Method, *Trans.ASME*, vol.57, pp.906-915,1990
12) Nakagawa, K. , Kitahara, M. and Hamada, M. : Application of Boundary Integral Equation Methods to Three Dimensional Elastodynamics, *Japan Nat. Symp. BEM*, 1, pp.163-168, 1984.
13) Tanaka, M. and Tanaka, K. : The Boundary Element Method - Introduction and Applications, Maruzen, 1992.
14) Tanaka, M. and Matsumoto, T. : The Boundary Element Method and Application, Baihukan, 1991.
15) Yamada, Y. and Hayami, K. : A Multi-pole Method for Two Dimensional Elastostatics, *BEM Technology Conference*, 5, pp.59-64, 1995.
16) Watanabe, O. and Hayami, K. : A Fast Solver for the Boundary Element Method using Multi-pole Expansion, *BEM Technology Conference*, 4 , pp.39-44, 1994, (in Japanese).
17) Fukui, T. , Hattori, J. and Doino, M. : Application of Fast Multi-pole Algorithm in Boundary Element Method, *Journal of Structural Mechanics*, vol.43A, pp.373-382, 1997.
18) Fukui, T. and Inoue, K. : Fast Multi-pole Boundary Element Method in 2D Elastdynamics, *Journal of Applied Mechanics*, vol.1, pp.373-380, 1998.
19) Washidu, H. , Miyamato, H. , Yamada, Y. , Yamamoto, Y. and Kawai ,T. : The Hand Book of the Fintite Element Method 2 for Application, Baihukan, 1983.

(Received June 23, 1999)

都市強震動予測のためのマクローミクロ解析

市村　強・堀　宗朗

都市域での強震動分布を数値計算するには，膨大な計算量と地盤情報の不確実性という二つの難点がある．これを解決するために，1) 階層型解析のための特異摂動と 2) バウンディング・メディア理論に基づいて地盤情報の不確実性に応じた幅をもって強震動分布を計算するマクロ-ミクロ解析を提案した．本論文では，定式化とプロトタイプの開発を行った．実際の地震について簡単なシミュレーションを行い，実測データと比較した．時間分解能 5[Hz]，空間分解能 2[m] という高分解能の計算が可能となり，マクロ - ミクロ解析の基本的な妥当性と有効性が検証されたと考えられる．